Journal of Volcanology and Geothermal Research 295 (2015) 16–25

Contents lists available at ScienceDirect

Journal of Volcanology and Geothermal Research

journal homepage: www.elsevier.com/locate/jvolgeores

New geochemical and isotopic insights to evaluate the geothermal resource of the hydrothermal system of Rosario de la Frontera (Salta, northern Argentina)

A. Chiodi [a], F. Tassi [b,c,*], W. Báez [a], R. Maffucci [d], C. Invernizzi [e], G. Giordano [d,e], S. Corrado [d], G. Bicocchi [b], O. Vaselli [b,c], J.G. Viramonte [a], P.P. Pierantoni [f]

[a] GEONORTE INENCO (UNSa—CONICET), Av. Bolivia 5150, A4400FVY Salta, Argentina
[b] Department of Earth Sciences, University of Florence, Via La Pira 4, 50121 Firenze, Italy
[c] CNR-IGG Institute of Geosciences and Earth Resources, Via La Pira 4, 50121 Firenze, Italy
[d] Department of Sciences, University Roma Tre, 00146 Roma, Italy
[e] CNR-IDPA Institute for Dynamics of Environmental Processes, Via M. Bianco, 20131 Milano, Italy
[f] School of Sciences and Technologies, University of Camerino, Via Gentile III da Varano, 62032 Camerino, Italy

ARTICLE INFO

Article history:
Received 27 November 2014
Accepted 3 March 2015
Available online 8 March 2015

Keywords:
Salta Region
Geothermal resource
Water geochemistry
Hydrothermal system
Thermal spring

ABSTRACT

In this study, the chemical and isotopic composition of thermo-mineral springs from the Rosario de la Frontera hydrothermal system was used to construct a conceptual model describing the source regions the thermal fluids and the chemical–physical processes controlling the chemistry of waters and dissolved gases during their underground circulation. The main hydrothermal reservoir, hosted within the Cretaceous Pirgua Subgroup deposits, is fed by meteoric water and shows a Na–HCO_3 composition produced by water–rock interactions involving sedimentary formations mostly consisting of conglomerates and sandstones, which are interbedded with alkaline volcanic rocks and shales and limestone deposits. This aquifer also receives significant contributions of crustal CO_2 and He from mantle degassing, the latter being likely favored by the regional tectonic assessment that is characterized by a deep detachment (at about 10 km depth) in the basement of the Santa Bárbara thick-skinned thrust system and a thinned lithosphere. The uprising thermal fluids mix with a relatively high salinity Na–Cl dominated aquifer produced by the interaction of meteoric water with the Tertiary Anta Formation evaporite. The temperatures of the hydrothermal reservoir, estimated with water geothermometers, are up to 130 °C, which are consistent with the thickness of the hydrothermal circuit (2700–3000 m) and the relatively high local geothermal gradient (~40 °C/km). These results suggest that the heat stored in the fluid phase of RFHS is up to ~1×10^{18} J, a value significantly higher (20%) than that previously estimated assuming an average reservoir temperature of 90 °C.

1. Introduction

Rosario de la Frontera (25°50′S–64°55′W; Salta Province, northern Argentina) is part of the Subandean foreland thrust belt, an area characterized by a geothermal gradient higher than the average value in the crust (~30 °C/km). In this area, numerous thermal springs occur, representing an important touristic attraction since 1880. Geophysical and hydrogeological investigations (Moreno Espelta et al., 1975; Seggiaro et al., 1995, 1997; Barcelona et al., 2013; Invernizzi et al., 2014) have shown that the Rosario de la Frontera thermal manifestations are fed by a hydrothermal system (Rosario de la Frontera Hydrothermal System, hereafter RFHS) that consists of two main aquifers at ~2400 and 150 m depth, respectively. A preliminary evaluation for the volume of the deepest aquifer, hosted within Cretaceous sedimentary units, accounts for 53 km^3 (Maffucci et al., 2012, 2013). A subsequent conservative evaluation (Invernizzi et al., 2014) suggested a reservoir volume of about 39 km^3. Invernizzi et al. (2014) also provided a preliminary evaluation of the RHFS geothermal potential, accounting for Er = 5.6×10^{18} J (heat stored in the solid rocks) and Ef = 0.8×10^{18} J (heat stored in the fluid phase). Despite the important energy potential of this natural resource, the geochemical features of the RFHS fluids have not been exhaustively investigated. This paper presents new chemical and isotopic data of waters and gases collected in October 2011 and April 2013 from 13 thermal discharges (hot springs and bubbling pools with temperatures up to 90.5 °C) located near the Rosario de la Frontera thermal spa. The main aim was to investigate the source regions of thermal fluids and provide

* Corresponding author at: Department of Earth Sciences, University of Florence, Via La Pira 4, 50121 Firenze, Italy. Tel.: +39 0552757477; fax: +39 0552284571.
E-mail address: franco.tassi@unifi.it (F. Tassi).

http://dx.doi.org/10.1016/j.jvolgeores.2015.03.001
0377-0273/

insights into the chemical–physical conditions of the hydrothermal reservoir for a reliable estimation of this thermal resource.

2. Geodynamic and stratigraphic settings

The RFHS is located in the northern sector of the La Candelaria range (hereafter LCR) that is part of the Santa Bárbara thick-skinned thrust system (hereafter SBS). The latter pertains to the N–S foreland thrust belt system produced in response to the Miocene Andean compressive phase (Fig. 1a) that caused the selective inversion of the Cretaceous normal faults (Bianucci et al., 1982; Allmendinger et al., 1983; Jordan et al., 1983; Grier et al., 1991; Salfity et al., 1993; Kress, 1995; Allmendinger and Gubbels, 1996; Cristallini et al., 1997; Kley and Monaldi, 1998, 2002; Reynolds et al., 2000; Carrera et al., 2006). LCR represents the structural framework of the RFHS and consists of broad anticlines N–S elongated and strongly plunging both to the north and to the south. The Termas anticline, located in the northern sector of the LCR, is uplifted by high angle reverse fault planes (Seggiaro et al., 1997) dipping both to the west and to the east with top-to-the-east and top-to-the-west sense of transport, respectively (Maffucci et al., 2013). Three major units characterize the stratigraphic succession at LCR (Fig. 1b): (i) the pre-rift sequence, (ii) the rift-related sedimentary/volcanic sequence and (iii) the synorogenic sequence. The pre-rift sequence consists of a fractured low-grade metasedimentary basement (Medina Formation, Late Proterozoic to Middle Cambrian; Bossi, 1969; Ramos, 2008), unconformably overlaid by the rift related sedimentary/volcanic sequence (Cretaceous to Paleogene Salta Group). The latter consists of three subgroups: (i) Pirgua, (ii) Balbuena and (iii) Santa Bárbara (Reyes and Salfity, 1973; Salfity and Marquillas, 1994). The Pirgua Subgroup (Early to Late Cretaceous), representing the syn-rift stage (Galliski and Viramonte, 1988; Salfity and Marquillas, 1994; Marquillas et al., 2005), mainly consists of red continental conglomerates and sandstones locally interbedded with alkaline volcanic rocks (Galliski and Viramonte, 1988). The Balbuena Subgroup (Latest Cretaceous to Early Paleocene) shows continental to restricted marine sandstones, limestones and shales (Turner, 1959). The Santa Bárbara Subgroup (Paleocene to Early Eocene) consists of shales with rare carbonate intercalations. The latest two units were related to the post-rift thermal subsidence stage (Bianucci et al., 1981; Gómez Omil et al., 1989; Comínguez and Ramos, 1995; Cristallini et al., 1997). The synorogenic sequence (Oran Group; Middle Miocene to Pleistocene) comprises two subgroups: i) The Metán Subgroup (Neogene), outcropping in the northern sector of LCR, dominated by sandstone and limestone deposits and showing some evaporite intercalations (Gebhard et al., 1974); ii) the Jujuy Subgroup (Late Miocene to Early Pleistocene) consisting of sandstones and conglomerates deposits (Gebhard et al., 1974; Mingramm et al., 1979; Galli et al., 1996; Hain et al., 2006).

3. Hydrogeological features of RFHS

Pirgua Subgroup, whose estimated permeability was of 83–95 mD (Invernizzi et al., 2014), is considered the main hydrothermal reservoir in the studied area (Moreno Espelta et al., 1975; Seggiaro et al., 1997). The low permeability sediments belonging to the Balbuena and Santa Barbara Subgroups likely act as a cap rock. The reservoir is hydraulically confined at depth by the Medina Formation, whose main lithotypes predominantly consist of impervious phyllites and quartzite with low permeability (Invernizzi et al., 2014 and references therein). Meteoric water permeating at depth from the northern sector of LCR, mainly through ENE–WSW and NNW–SSE oriented fault systems (Fig. 1b), likely represents the main recharge source for RHFS. These fault systems also control the spatial distribution of the thermal fluid discharges (Fig. 2a) (Seggiaro et al., 1997; Pesce and Miranda, 2003; Invernizzi et al., 2014). For this hydrothermal system, preliminary geothermometric calculations based on the chemistry (K^+/Mg^{2+} ratios) of some thermal waters (Seggiaro et al., 1995) indicated a geothermal gradient up to 43.3 °C/km, whereas organic and inorganic paleo-thermal indicators (Di Paolo et al., 2012) suggested a slightly lower value (~40 °C/km).

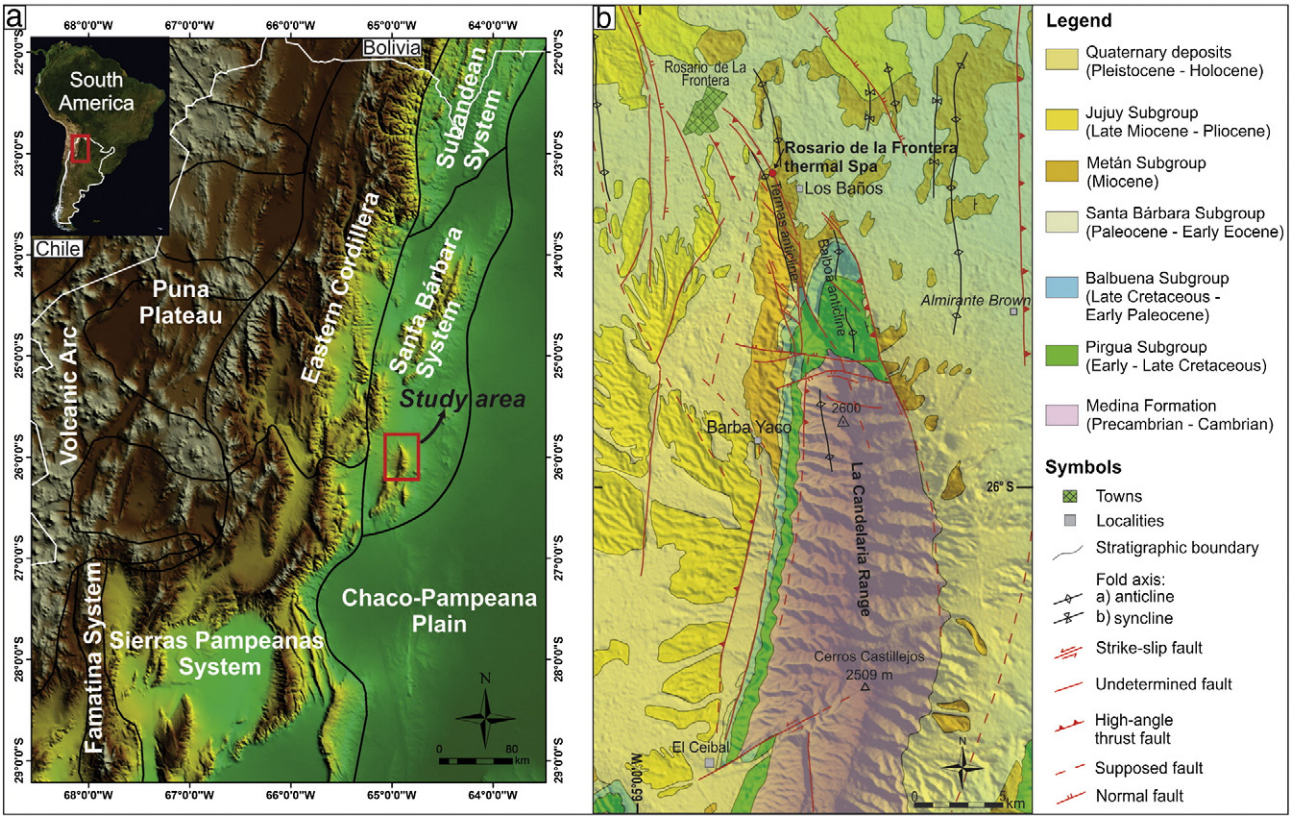

Fig. 1. (a) Location of the study area and (b) geological map of the northern sector of La Candelaria Range (modified from Maffucci et al., 2013).

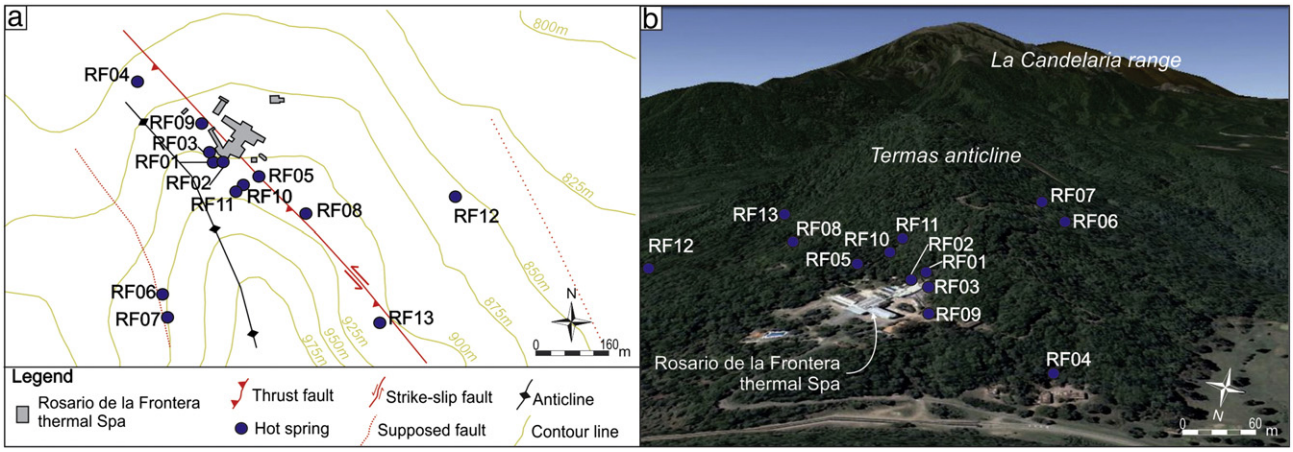

Fig. 2. (a) Morphotectonic map of the Termas anticline and (b) 3D-image of the studied area (from Google Earth). Both maps report the location of the sampling sites.

4. Materials and methods

4.1. Chemical and isotopic ($\delta^{18}O$–H_2O, $\delta^{2}H$–H_2O, $\delta^{11}B$ and $\delta^{34}S$–SO_4) analysis of water samples

Water samples were collected from hot springs located in a small area (~0.56 km^2) along the flanks of the Las Termas anticline (Fig. 2a, b). Temperature (°C), pH values, and alkalinity (analyzed by acidimetric titration with 0.01 N HCl and methyl-orange as indicator) were measured in the field (Table 1). At each sampling point, two water aliquots, one acidified with suprapur HCl, were filtered at 0.45 μm and stored in high-density polyethylene bottles. Laboratory analyses for major cations (Na^+, K^+, Ca^{2+}, Mg^{2+}, Li^+, and NH_4^+) and anions (Cl^-, SO_4^{2-}, NO_3^-, Br^- and F^-) were carried out by ion-chromatography (IC: Metrohm 861 and 761, respectively). The analysis of B was carried out following the Azometina-H method (AH; Bencini, 1985), whereas SiO_2 was analyzed, on water samples diluted (1:10) in situ, by molecular spectrophotometry (MS) after the addition of a 10% (*w*/*v*) ammonia molybdate solution in a sulfuric acid environment. The errors for the IC, HS and MS analysis were ≤5%.

The $^{18}O/^{16}O$ ratios of H_2O (expressed as $\delta^{18}O$–H_2O ‰ vs. V-SMOW) were analyzed by using a Finnigan Delta Plus XL mass spectrometer according to the CO_2–H_2O equilibration method proposed by Epstein and Mayeda (1953). The $^{2}H/^{1}H$ ratios of H_2O (expressed as $\delta^{2}H$-H_2O ‰ vs. V-SMOW) were analyzed on H_2 after the reaction of 10 mL of water with metallic zinc at 500 °C (Coleman et al., 1982). The analytical errors for $\delta^{18}O$–H_2O and $\delta^{2}H$–H_2O values were ±0.1‰ and ±1‰, respectively.

The $^{34}S/^{32}S$ ratios of SO_4^{2-} (expressed as $\delta^{34}S$–SO_4‰ vs. V-CDT) were analyzed using an EA-IRMS system consisting of a 20–20 isotope ratio mass spectrometer (Europa Scientific, Crewe, UK), equipped with an elemental analyser (Sercon Ltd, Crewe, UK), after the precipitation of $BaSO_4$ with a $BaCl_2$ solution. The solid was separated by centrifugation, dried and transferred into tin capsules, which were combusted at ≈1700 °C, to form, among the other gases, SO_2. Then, SO_2 was separated on a packed GC column at 45 °C. The isotopic analysis was based on monitoring of m/z 48, 49 and 50 of SO^+ produced from SO_2 in the ion source. The analytical uncertainly was ±0.3‰.

The $^{11}B/^{10}B$ ratios (expressed as $\delta^{11}B$‰), were analyzed on selected samples by MC-ICP-MS (NEPTUNE, Thermo-Scientific; 2σ ≤ 0.77‰) at ALS Laboratories (Sweden). Prior to the isotopic analysis, 100 to 150 mL of water were pre-concentrated using the boron specific ion-exchange resin Amberlite IRA 743 in order to have about 100 μg/L of boron in solution (Aggarwal et al., 2009).

4.2. Sampling and chemical analysis of gas samples

Dissolved gases were collected from 10 thermal springs (Table 2) using pre-evacuated 250 mL pyrex flasks equipped with Thorion® stopcock and filled with water up to about 3/4 of their inner volume (Tassi et al., 2008). One free gas sample was collected from the RF02 bubbling pool (Table 2) using a pre-evacuated 60 mL glass thorion-tapped flask filled with 20 mL of a 4 N NaOH solution (Giggenbach and Goguel, 1989; Vaselli et al., 2006).

Inorganic gases (N_2, O_2, H_2, Ar, and He) in the headspace of the sampling flask used for the bubbling gas, as well as those collected in the headspace of the dissolved gas vials (N_2, O_2, H_2, Ar, He, CO_2 and H_2S), were analyzed by gas chromatography (GC). The GC (Shimadzu 15A), equipped with a thermal conductivity detector TCD, was assembled with a (i) 10 m long 5A molecular sieve column and a (ii) 3 m long column packed with Porapak Q 80/100 mesh for the analysis of the bubbling gas and the dissolved gases, respectively. Carbon dioxide and H_2S in the alkaline solution of the bubbling gas flask were analyzed as CO_3^{2-} (by titration with a 0.5 N HCl solution) and SO_4^{2-} (by ionic chromatography, IC, after oxidation with H_2O_2), respectively. Light hydrocarbons, including CH_4, were analyzed using a Shimadzu 14A GC equipped with a 10 m long stainless steel column (ϕ = 2 mm) packed with Chromosorb PAW 80/100 mesh coated with 23% SP 1700 and a Flame Ionization Detector (FID). The analytical errors for titration, GC and IC analyses were <5%.

The $^{13}C/^{12}C$ ratios of dissolved CO_2 (expressed as $\delta^{13}C$–CO_2 ‰ vs. V-PDB) were computed from the $\delta^{13}C$ values measured in CO_2 of the flask headspace ($\delta^{13}C$–CO_{2STRIP}), using the ε_1 factor for gas–water isotope equilibrium proposed by Zhang et al. (1995), as follows:

$$\varepsilon_1 = \delta^{13}C\text{-}CO_2\ \delta^{13}C\text{-}CO_{2STRIP} = 0.0049 \times T(^{\circ}C)\ 1.31 \quad (1)$$

The $\delta^{13}C$–CO_{2STRIP} analyses were carried out with a Finningan Delta S mass spectrometer after extracting and purifying CO_2 by using liquid N_2 and N_2-trichloroethylene cryogenic traps (Evans et al., 1998; Vaselli et al., 2006). The $^{13}C/^{12}C$ ratios of CO_2 of the bubbling gas flask were measured by using 2 mL of the soda solution after the addition of ~5 mL of anhydrous phosphoric acid for the extraction of CO_2. Isotopic equilibration was achieved in a thermal bath at the temperature of 25 ± 0.1 °C for at least 8 h. The extracted CO_2 was treated as previously described for the CO_{2STRIP}. The $^{13}C/^{12}C$ ratios were analyzed with a Finningan Delta S mass spectrometer. Internal (Carrara and San Vincenzo marbles) and international (NBS18 and NBS19) standards were used for estimating the external precision. The analytical uncertainty and the reproducibility were ±0.05‰ and ±0.1‰, respectively. The $^{13}C/^{12}C$ ratios of CH_4 (expressed as $\delta^{13}C$–CH_4 ‰V-PDB) were analyzed by mass spectrometry (Varian MAT 250) according to the procedure reported by Schoell (1980). The analytical uncertainly was ±0.15‰.

The $^{3}He/^{4}He$ ratios (expressed as R/Ra, where R is the $^{3}He/^{4}He$ measured ratio and Ra is the $^{3}He/^{4}He$ ratio in the air: 1.39 10^{-6}; Mamyrin and Tolstikhin, 1984) were determined by using a double collector

Table 1
Outlet temperatures (in °C), pH, chemical composition, $\delta^{34}S–SO_4$ (expressed as ‰ vs. V-CDT), $\delta^{18}O$ and $\delta^{2}H$ (both expressed as ‰ vs. V-SMOW) and $\delta^{11}B$ (in ‰) values of the RFHS fluid discharges. Concentrations of solutes are in mg/L; n.a.: not analyzed. * data from Invernizzi et al. (2014).

	Latitude	Longitude	Altitude	T	pH	HCO_3^-	F^-	Cl^-	Br^-	NO_3^-	SO_4^{2-}	Ca^{2+}	Mg^{2+}	Na^+	K^+	NH_4^+	B	SiO_2	$\delta^{34}S–SO_4$	$\delta^{18}O–H_2O$	$\delta D–H_2O$	$\delta^{11}B$
RF01	25.84	64.93	924	74.0	6.75	169	2.3	313	0.1	0.6	128	11	0.5	305	4.3	0.05	0.12	92	n.a.	−7.0	−38	
RF02	25.84	64.93	905	81.2	6.88	156	1.8	682	0.2	0.5	190	10.6	0.5	587	7.4	0.06	0.18	88	6.99	−6.9	−38	
RF03	25.84	64.93	918	71.4	7.06	201	8.8	16000	2.1	0.1	2100	326	20.1	11200	80.8	0.07	0.23	47	n.a.	−7.1	−40	0.87
RF04	25.84	64.93	865	24.1	6.84	315	8.7	5340	2	6.1	3010	440	63.5	4290	17.4	0.05	0.33	54	6.31	−6.4	−38	1.05
RF05	25.84	64.93	948	52.7	6.42	198	1.9	137	0.2	1.2	146	32	1.5	188	2.7	0.05	0.21	94	n.a.	−6.8	−37	
RF06	25.84	64.93	960	64.8	6.09	149	0.7	270	0.2	1.4	104	5.1	0.1	288	4.0	0.07	0.39	89	n.a.	−6.6	−36	
RF07	25.84	64.93	967	58.2	6.73	224	2.5	42	0.1	1.5	103	15	0.7	147	1.7	0.13	0.27	85	n.a.	−6.6	−36	13.8
RF08	25.84	64.93	954	74.9	6.83	219	1.5	122	0.1	1	143	22	0.9	193	2.3	0.07	0.15	87	5.87	−6.6	−37	
RF09	25.84	64.93	894	24.2	7.36	279	1.5	2510	1.6	2.7	626	75	10.9	1900	17.4	0.11	0.45	51	5.42	−6.6	−38	
RF10	25.84	64.93	928	90.5	6.12	171	2.5	276	0.2	0.2	187	3.9	0.2	321	5.7	0.09	0.28	102	7.32	−6.9	−39	12.6
RF11	25.84	64.93	942	90.4	6.39	190	8.0	254	0.2	0.9	180	14	0.3	294	5.6	0.28	0.35	108	n.a.	−6.5	−36	
RF12	25.84	64.93	867	45.2	6.77	215	2.3	80	0.1	0.3	155	4.6	0.28	206	4.7	0.26	0.44	116	n.a.	−6.6	−36	
RF13	25.84	64.93	918	72.2	6.26	210	2.0	133	0.1	0.4	140	3.2	0.1	227	5.3	0.20	0.51	124	n.a.	−6.5	−37	

Table 2
Chemical composition, $\delta^{13}C$ in CO_2 and CH_4 (both expressed as ‰ vs. V-PDB) and R/Ra values of the bubbling and dissolved gases from the RFHS. Concentrations are in mmol/mol; n.d.: not detected.

Sample	type	CO_2	H_2S	N_2	CH_4	Ar	O_2	Ne	H_2	He	C_2H_6	C_3H_8	i-C_4H_{10}	n-C_4H_{10}	i-C_4H_8	i-C_5H_{12}	n-C_5H_{12}	C_6H_6	$\delta^{13}C–CO_2$	R/Ra	$\delta^{13}C–CH_4$
RF01	dissolved	209	n.d.	756	0.011	17.4	18	0.0093	n.d.	0.0015	n.d.	n.d.	n.d.	n.d.	n.d.	n.d.	n.d.	n.d.	−6.56		
RF02	bubbling	956	3.6	28	0.051	0.59	12	0.0003	0.015	0.0044	0.00061	0.00005	0.00004	0.00003	0.00003	0.00002	0.00003	0.00011	−4.11	1.15	−39.3
RF03	dissolved	168	n.d.	803	0.005	16.9	12	0.009	n.d.	0.0021	n.d.	n.d.	n.d.	n.d.	n.d.	n.d.	n.d.	n.d.	−7.13		
RF04	dissolved	139	n.d.	841	0.087	19	2.3	0.010	n.d.	0.0011	n.d.	n.d.	n.d.	n.d.	n.d.	n.d.	n.d.	n.d.	−5.66		−41.5
RF05	dissolved	575	n.d.	385	0.011	8.9	31	0.005	n.d.	0.0061	n.d.	n.d.	n.d.	n.d.	n.d.	n.d.	n.d.	n.d.	−5.16		
RF06	dissolved	889	n.d.	106	0.051	2.39	2.66	0.0015	n.d.	0.0021	0.00061	0.00002	0.00003	0.00002	0.00005	0.00003	0.00002	0.00018	−4.15		−41.4
RF08	dissolved	212	n.d.	755	0.115	18.5	14	0.010	n.d.	0.0013	n.d.	n.d.	n.d.	n.d.	n.d.	n.d.	n.d.	n.d.	−11.49		
RF09	dissolved	296	n.d.	676	0.009	17.1	11	0.009	n.d.	0.0024	n.d.	n.d.	n.d.	n.d.	n.d.	n.d.	n.d.	n.d.	−4.11		
RF10	dissolved	960	1.2	36	0.087	0.77	2.3	0.0004	0.011	0.0042	0.00077	0.00004	0.00005	0.00002	0.00004	0.00002	0.00003	0.00015	−3.66	0.98	−40.6
RF11	dissolved	550	n.d.	415	0.015	9.8	25	0.006	n.d.	0.0027	n.d.	n.d.	n.d.	n.d.	n.d.	n.d.	n.d.	n.d.	−4.44		
RF13	dissolved	954	n.d.	44	0.069	0.89	1.5	0.0005	0.022	0.0033	0.00078	0.00003	0.00002	0.00004	0.00006	0.00003	0.00004	0.00021	−3.77		−39.8

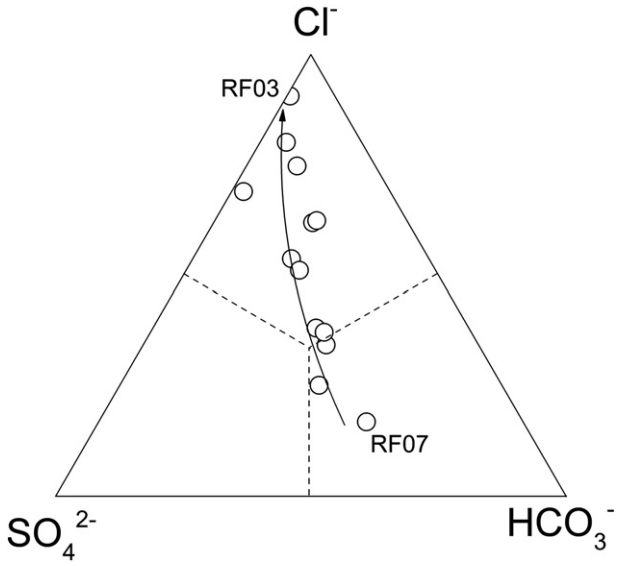

Fig. 3. SO_4^{-2}–Cl^-–HCO_3^- ternary diagram (in meq/L) for the RFHS fluid discharges.

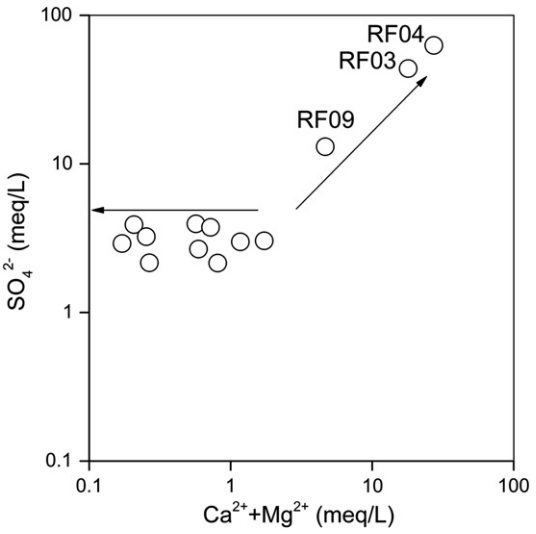

Fig. 5. SO_4^{2-} vs. ($Ca^{2+}+Mg^{2+}$) binary diagram (in meq/L) for the RFHS fluid discharges.

mass spectrometer (VG 5400-TFT) according to method described by Inguaggiato and Rizzo (2004). The analytical uncertainty was ±1%.

5. Results

5.1. Chemical and isotopic compositions of waters

Temperature, pH and chemical composition of the thermal springs are reported in Table 1. Water temperatures ranged from 24.1 (RF04) to 90.5 °C (RF10), whereas the pH values were from 6.09 (RF06) to 7.36 (RF09). The TDS (Total Dissolved Solids) were relatively low (TDS <1,050 mg/L), with the exception of those of the RF03, RF04 and RF09 samples (from 5400 to 30,000 mg/L). Most collected waters showed a Na^+–Cl^-(SO_4^{2-}) composition, with the exception of the RF07 and RF12 samples that had a Na^+–HCO_3^- composition. The Na^+ concentrations (up to 11,200 mg/L) were consistently 1–2 orders of magnitude higher than those of the other cations. On the contrary, the relative concentrations of the main anions were largely variable, as shown by the HCO_3^-/Cl^- and SO_4^{2-}/Cl^- molar ratios that ranged from 0.007 to 3.11 and from 0.09 to 1.82, respectively. Silica concentrations varied in a relatively wide range (from 47 to 124 mg/L), while F^-, Br^- and B concentrations did not exceed 8.8, 2.08 and 0.51 mg/L, respectively. N-bearing compounds were dominated by NO_3^- (from 0.22 to 6.13 mg/L), with relatively low concentrations of NH_4^+ (<0.28 mg/L).

The $\delta^{34}S$–SO_4 values, measured in 5 selected water samples (RF02, RF04, RF08, RF09 and RF10), were from 5.42‰ and 7.32‰ vs. V-CDT (Table 1). The RF07 and RF10 showed similar ^{11}B values (13.8‰ and 12.6‰ vs. NBS H_3BO_3 951, respectively), whereas those of RF03 and RF04 are significantly lower (0.87‰ and 1.05‰, respectively). The $\delta^{18}O$–H_2O, δ^2H–H_2O values, which were already reported by Invernizzi et al. (2014), clustered in relatively narrow ranges, from −7.1‰ to −6.4‰ and from −40‰ to −36‰ vs. V-SMOW, respectively (Table 1).

5.2. Chemical and isotopic compositions of gases

The chemical composition of dissolved gases and that of the RF02 bubbling gas are reported in Table 2 (in mmol/mol). The dissolved gas composition was calculated from the analytical data of the gases stored in the headspace of the sampling glass flasks on the basis of i) gas pressure, ii) headspace volume and iii) the solubility coefficients of each gas compound (Whitfield, 1978).

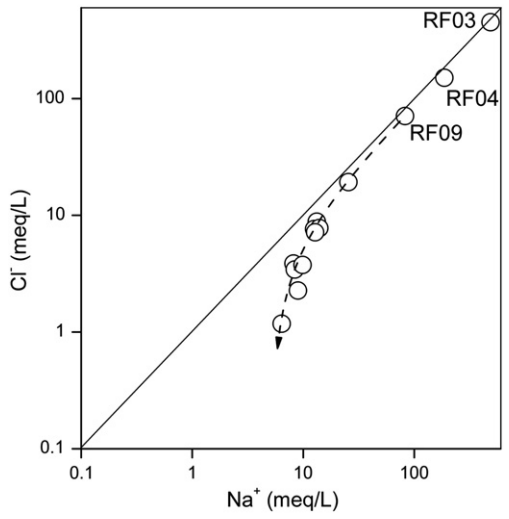

Fig. 4. Cl^- vs. Na^+ binary diagram (in meq/L) for the RFHS fluid discharges. The Na^+–Cl^- stoichiometric line is also reported.

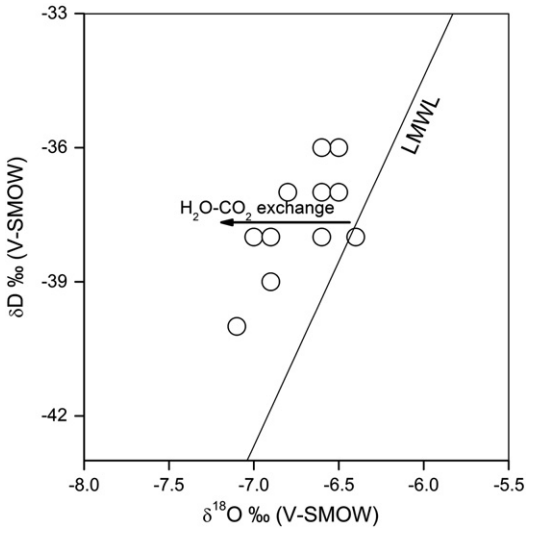

Fig. 6. δD vs. $\delta^{18}O$ binary diagram for the RFHS fluid discharges. The Local Meteoric Water Line (LMWL: $\delta^2H‰ = (8.25 \pm 0.18) \times \delta^{18}O‰ + (15.08 \pm 0.96)$; Dapeña and Panarello, 2011) is also reported.

Table 3
Saturation indexes of calcite, dolomite, gypsum, halite, fluorite and chalcedony for the RFHS fluid discharges. Calculations were carried using the PHREEQC v. 3.2 (Parkhurst and Appelo, 1999) software package (llnl database).

	Calcite	Dolomite	Gypsum	Halite	Fluorite	Chalcedony
RF01	−0.83	−1.50	−2.28	−5.66	−1.91	−0.08
RF02	0.81	−1.48	−1.95	−4.86	−2.56	0.06
RF05	−0.82	−1.52	−1.81	−6.21	−1.53	0.17
RF06	−1.98	−4.04	−2.72	−5.74	−3.22	0.04
RF07	−0.38	−2.15	−2.31	−6.45	−3.91	0.03
RF08	−0.29	−0.53	−1.89	−6.26	−1.95	−0.11
RF10	−1.70	−3.39	−2.52	−5.70	−2.32	−0.18
RF11	−0.83	−1.99	−1.98	−5.77	−0.75	−0.16
RF12	−1.66	−3.05	−2.61	−6.21	−2.51	0.02
RF13	−1.72	−3.37	−2.75	−6.15	−2.53	0.08

The composition of the bubbling gas (RF02), as well as that of some dissolved gas samples (RF06, RF10, and RF13) was dominated by CO_2 (from 889 to 960 mmol/mol) and subordinate concentrations of N_2 (up to 106 mmol/mol), CH_4 (from 0.051 to 0.087 mmol/mol), O_2 (up to 12 mmol/mol), Ar (up to 2.39 mmol/mol), and He (from 0.0021 to 0.0044 mmol/mol). In these CO_2-rich gases, H_2S (3.6 and 1.2 mmol/mol in RF2 and RF10, respectively), H_2 (up to 0.022 mmol/mol), and light hydrocarbons (whose sum was up to 0.0012 mmol/mol) were also measured. RF01, RF03, RF04, RF08 and RF09 dissolved gases showed relatively high concentrations of N_2 (from 676 to 841 mmol/mol) and Ar (from 16.9 to 18.6 mmol/mol), with variable concentrations of O_2 (from 2.3 to 18 mmol/mol) and CH_4 (from 0.005 to 0.115 mmol/mol). In these samples, CO_2 concentrations were relatively low (up to 296 mmol/mol), whereas H_2S, H_2 and light hydrocarbons were not detected. The RF05 and RF11 dissolved gases showed an intermediate composition, being characterized by comparable concentrations of CO_2 and N_2 (up to 575 and 415 mmol/mol, respectively), Ar and CH_4 up to 9.8 and 0.015 mmol/mol, and high O_2 concentration (31 and 25 mmol/mol, respectively).

The $\delta^{13}C$–CO_2 values ranged from −11.49‰ to −3.66‰ vs. V-PDB, whereas those of $\delta^{13}C$–CH_4, which were measured in selected samples (RF02, RF04, RF06, RF10 and RF13) were comprised between −41.5‰ and −39.3‰ vs. V-PDB. The R/Ra values of RF02 and RF10, corrected for air contamination according to the measured He/Ne ratios (Sano and Wakita, 1985), were relatively low (0.98 and 1.15, respectively).

6. Discussion

6.1. Processes controlling the chemistry of waters

The relative concentrations of the main anions (Fig. 3) suggest that the chemistry of the RFHS waters is controlled by mixing of highly saline Cl^-(SO_4^{2-})-rich fluids, such as those discharged from RF03, with waters, whose end-member is likely represented by the RF07 sample, which shows a relatively low TDS and a Na^+–HCO_3^- composition. Dissolution of halite and gypsum, both largely occurring in the evaporites of the Anta Formation (Galli and Hernández, 1999), is responsible for the relatively high Na^+–Cl^- (Fig. 4) and Ca^{2+}, Mg^{2+} and SO_4^{2-} (Fig. 5) concentrations of the RF03-type waters (RF03, RF04 ad RF09). Accordingly, the $\delta^{34}S$-SO_4 values (Table 1) were consistent with those measured in Neogene to Recent gypsum deposit, such as those recognized in the Salar de Atacama basin (northern Chile) that range from 3.0‰ to 7.6‰ vs. V-CDT (Spiro and Chong, 1996; Carmona et al., 2000; Cortecci et al., 2005; Leybourne et al., 2013). The Na^+/Cl^- molar ratios (>1) of the RF07-type waters (Fig. 4), which are not consistent with halite dissolution, were likely produced by leaching of Na-silicates, such as feldspars and their alteration products (illite), which were recognized in conglomerates and sandstones of the Pirgua Subgroup (Marquillas et al., 2005). These waters also have relatively high $SO_4^{2-}/(Ca^{2+} + Mg^{2+})$ ratios (>4; Fig. 5), possibly due to SO_4^{2-} contribution from oxidation of H_2S, whose presence in association with CO_2 is testified by the gas composition of RF02 and RF10 (Table 2). The $\delta^{11}B$ values of the RF03-type waters (RF03 and RF04; Table 1) are in the range of those characterizing halite from evaporitic deposits in western Puna (Kasemann et al., 2004), whereas those of the RF07-type waters (RF07 and RF10; Table 1) are similar to that measured in the Cretaceous sediments from Central Andes (Fiedler, 2001). Therefore, the isotopic signature of B is consistent with the twofold origin of the RFHS fluid discharges as hypothesized on the basis of their chemical composition. The water isotopic data (Fig. 6)

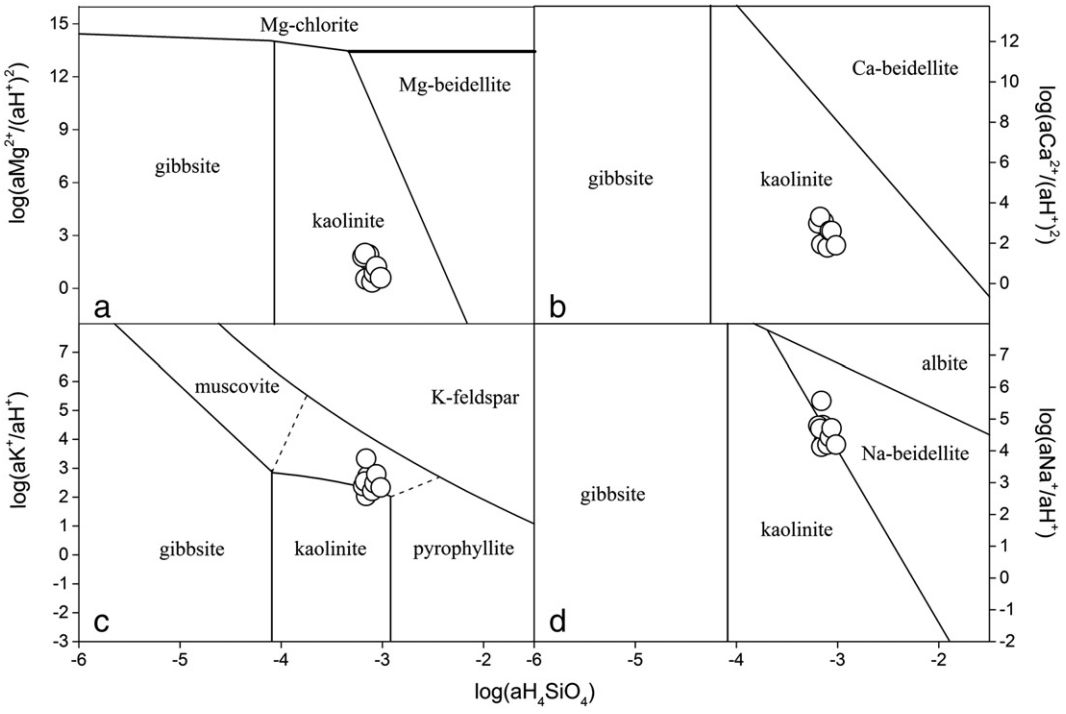

Fig. 7. (a) $\log(aMg^{2+}/(aH^+)$ vs. $\log(aH_4SiO_4)$, (b) $\log(aCa^{2+}/(aH^+)$ vs. $\log(aH_4SiO_4)$, (c) $\log(aK^+/(aH^+)$ vs. $\log(aH_4SiO_4)$, and (d) $\log(aNa^+/(aH^+)$ vs. $\log(aH_4SiO_4)$ binary diagrams for the RFHS fluid discharges.

indicate that the RFHS is fed by meteoric water, considering the average altitude of the recharge area (1680 m a.s.l.; Invernizzi et al., 2014) and the altitude vs. $\delta^{18}O$ relationship for the Andean regions (Gonfiantini et al., 2001). The slight negative ^{18}O-shift shown by the RF07-type waters respect to the Local Meteoric Water Line (LMWL; Dapeña and Panarello, 2011) is possibly due to H_2O–CO_2 isotopic exchange, a process that is efficient at relatively low temperatures (~100 °C; Chiodini et al., 2000). Summarizing, as highlighted by the geophysical measurements (Barcelona et al., 2013) and the hydrological models (Invernizzi et al., 2014, and references therein), the chemical and isotopic features of thermal discharges confirm that RFHS is characterized by the occurrence of two distinct aquifers, from the top to the bottom:

1) a Na^+–Cl^-(SO_4^{2-})-type aquifer, produced at shallow depth by interaction of meteoric water with highly soluble evaporitic deposits belonging to the Anta formation (Metán Subgroup). The highly saline waters recognized at Rosario de la Frontera (Fig. 1) (Bercheñi, 2003), ~2.4 km from the study area, are likely related to this source. Halite dissolution as the main Cl^- source is also supported by the high Cl^-/Br^- ratios (up to 7,700) of the RH03-type waters (Yardley and Bodnar, 2014). This evidence, coupled with the low B/Cl^- ratios (<0.011) and NH_4^+ concentrations (<0.28 mg/L), allows to exclude the presence of a deep geothermal brine (Tonani, 1970; Martini et al., 1984; Giggenbach, 1991; Arnósson and Andresdottir, 1995; Aggarwal et al., 2000).
2) a Na^+–HCO_3^- aquifer, representing the main hydrothermal reservoir in this area, fed by meteoric water, whose interaction with silicate minerals of the Pirgua Subgroup is likely favored by the presence of CO_2. Saturation indexes of the main minerals, computed using the PHREEQC v. 3.2 (Parkhurst and Appelo, 1999) software package (llnl database), show that the RF07-type waters are undersaturated with respect to calcite, dolomite, gypsum, halite and fluorite, and they are only slightly saturated in chalcedony (Table 3). Equilibrium activity (calculated on the basis of different ions and $SiO_{2(aq)}$ for each water sample) diagrams for coexisting minerals and aqueous solutions (the theoretical grids were computed at 25 °C and 1.013 bar; Fig. 7a–d) show that the RF07-type waters plot in correspondence of the fields of low temperature minerals (kaolinite, Na-beidellite and pyrophyllite).

6.2. Gas geochemistry

The $\delta^{13}C$–CO_2 values of the RFHS samples, with the exception of RF08 (Table 2), are consistent with those of CO_2 from mantle degassing (Javoy et al., 1982; Rollinson, 1993). However, the $CO_2/^3He$ ratios (up to 1.68×10^{11}) are two orders of magnitude higher than the MORB one (Marty and Jambon, 1987). This implies that CO_2 mainly derived from a crustal source: 1) degradation of organic matter and/or 2) thermometamorphic processes. The first hypothesis is unlike since organic CO_2 is characterized by $\delta^{13}C$–CO_2 values $\leq -20‰$ vs. V-PDB (Hoefs, 2008), i.e. too negative when compared to those of the RFHS samples. Similarly, the RFHS carbon isotopic signature seems to exclude a significant contribution of CO_2 produced by reactions involving limestone, which generally shows $\delta^{13}C$–CO_2 values between −2‰ and +2‰ vs. V-PDB (Rollinson, 1993). This apparent contradiction is likely due to the effects of secondary processes, such as (i) calcite precipitation producing ^{12}C-rich CO_2 and (ii) ^{13}C–^{12}C fractionation related to dissolution of gaseous CO_2 in the thermal waters. The R/Ra values (0.98 and 1.15) indicate a significant contribution (~12.2–14.3%) of mantle He (Poreda and Craig, 1989; Hilton et al., 2002). Occurrence of fluid contribution from such a deep source in the RFHS is likely favored by local tectonics since a deep detachment (at about 10 km depth) in the basement of the SBS and a thinned lithosphere was evidenced by Kley and Monaldi (2002) and Whitman et al. (1996), respectively. The relatively low N_2/Ar ratios, which are consistent with those of air saturated water (ASW: 38–42 at temperature between 20 and 70 °C), seem to exclude

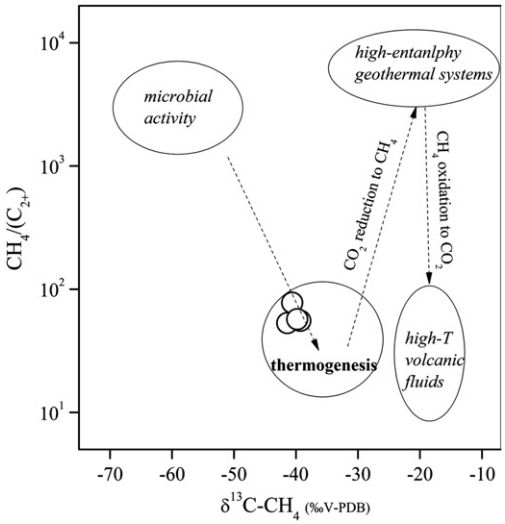

Fig. 8. $CH_4/(C_{2+})$ vs. $\delta^{13}C$–CH_4 diagram (modified from Tassi et al., 2012) for the bubbling gas (RF02) and dissolved gases (RF06, RF10 and RF13) of the RFHS fluid discharges.

the presence of N_2 from an extra-atmospheric source, such as microbial activity and/or thermogenic processes. Air dissolved in meteoric water recharging the hydrothermal aquifer is thus the main source for N_2, Ar, and Ne. The relatively large variability of the O_2/Ar ratios (from 0.12 to 20) suggests interaction processes, at different degrees, between emerging waters and air, since O_2 is basically absent at reducing conditions typical of hydrothermal reservoirs. The CH_4 concentrations are not related with those of the main gas compounds, i.e. CO_2 and N_2 (Table 2). This suggests that the origin of CH_4 is related to a process independent on the balance between deep fluids and air contribution. According to the CH_4/C_{2+} vs. $\delta^{13}C$–CH_4 binary diagram proposed by (Tassi et al. (2012), modified after Bernard et al., 1978), where C_{2+} is the sum of C_2–C_5 alkanes, hydrocarbons in the RFHS originated from thermogenic degradation of preexisting organic matter occurring at temperatures <150–200 °C (Fig. 8). The occurrence of H_2 in those samples showing detectable C_{2+} hydrocarbons provides the evidence that the organic gases were mostly produced within the hydrothermal aquifer, where these processes are favored by temperature and reducing conditions.

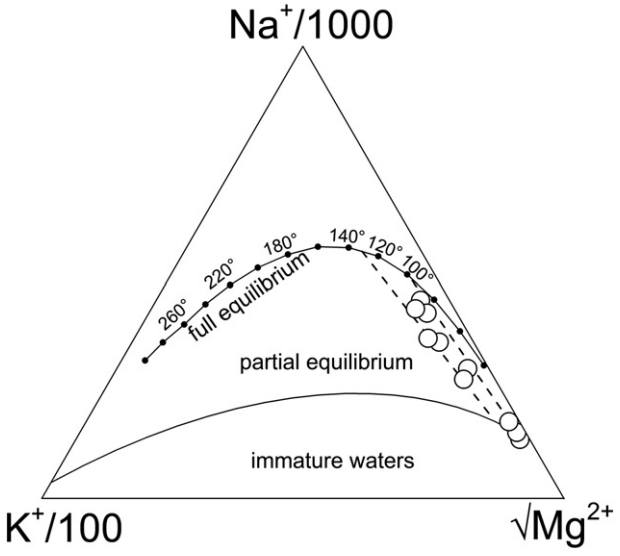

Fig. 9. $\sqrt{Mg^{2+}}$–$Na^+/1000$–$K^+/100$ triangular diagram (Giggenbach, 1988) for the RFHS fluid discharges. Curves for partial and full equilibrium are also reported.

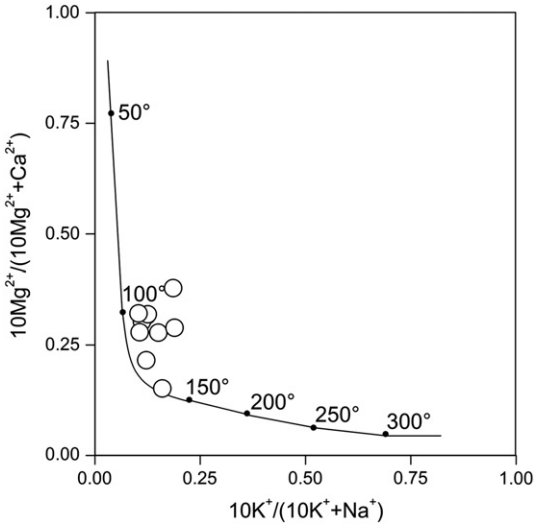

Fig. 10. $10 \times Mg^{2+}/(10 \times Mg^{2+} + Ca^{2+})$ vs. $10 \times K^{+}/(10 \times K^{+} + Na^{+})$ binary diagram. The expected composition of waters in equilibrium with an average crustal rock as a function of temperature (Giggenbach, 1988) is reported.

6.3. Geothermometry

A reliable evaluation of the temperatures at depth for the RFHS geothermal reservoir can be calculated on the basis of the equilibrium reactions in the Na–K–Mg–Ca system (Giggenbach, 1988, 1991). As shown in the Na/1000–K/100–√Mg ternary diagram (Fig. 9), the RFHS waters display a different degree of maturation and seem to point to the full equilibrium curve at 100–130 °C. Similar equilibrium temperatures are obtained when the 10 K/(10 K + Na) vs. 10 Mg/(10 Mg + Ca) diagram (Giggenbach, 1988; Fig. 10) is applied. For this computation, those waters (RF03, RF04 and RF09) with a Na^{+}–Cl^{-} composition and Cl^{-} concentrations >2500 mg/L, which strongly depend on the contribution from the saline shallow aquifer, were not considered. Equilibrium temperatures based on the solubility of chalcedony (Arnórsson, 1985) range from 100 to 122 °C, providing a further confirmation for the results obtained by applying the cation geothermometers. The relatively high temperatures (up to 90.5 °C; Table 1) measured at the outlet of some springs indicate that the discharging fluids are not significantly affected by conductive cooling. This is likely due to their high discharge rates (>2 m^3/h; thermal spa, pers. comm.). This feature can also justify the relatively high temperature (70.5 °C; Table 2) of the RF03 spring, whose chemistry indicates that it suffered the highest contamination by the shallow aquifer among the studied samples (Fig. 4). Nevertheless, a reliable estimation of the effects of the mixing process between the two aquifers based on the outlet temperatures cannot be computed, the temperature of the shallower one being unknown.

7. Conclusions

Two distinct aquifers can clearly be distinguished at RFHS on the basis of the chemical and isotopic compositions of the thermal discharges: a deep Na–HCO_3 reservoir, which represents the hydrothermal system, and a shallower Na^{+}–Cl^{-}(SO_4^{2-}) aquifer. The former is mainly recharged by meteoric water with the addition of crustal CO_2 and minor contribution from mantle degassing through the fault systems of LCR, as evidenced by the helium isotopic composition. The tectonic lineaments also control the uprising of hydrothermal fluids toward the surface during which they mix with the relatively shallow Na^{+}–Cl^{-}(SO_4^{2-}) waters deriving from interactions with shallow evaporitic deposits of the Anta Formation. Minor contributions of thermogenic organic gases were also recognized. A schematic conceptual model for the underground fluid circulation of RFHS is reported in Fig. 11. Estimations carried out using different geothermometers consistently indicate temperatures in the range of 100–130 °C for the deep hydrothermal reservoir and they likely represent the minimum expected temperatures. Considering a surface water temperature of 20 °C (Invernizzi et al., 2014) and the local geothermal gradient (~40 °C/km), recharging meteoric water can reach reservoir temperatures at 2100–2900 m depth, consistent with the difference between the average altitude of the recharge area (1680 m a.s.l.) and the depth of the Pirgua Subgroup (1100–1500 m b.s.l.). Assuming that the average reservoir temperature is ~115 °C, the preliminary evaluation of the energy potential of RFHS (heat stored in the fluid phase: 0.8×10^{18} J; Invernizzi et al., 2014), calculated on the basis of a fluid temperature of 90 °C, is to be considered significantly (~20%) underestimated. These

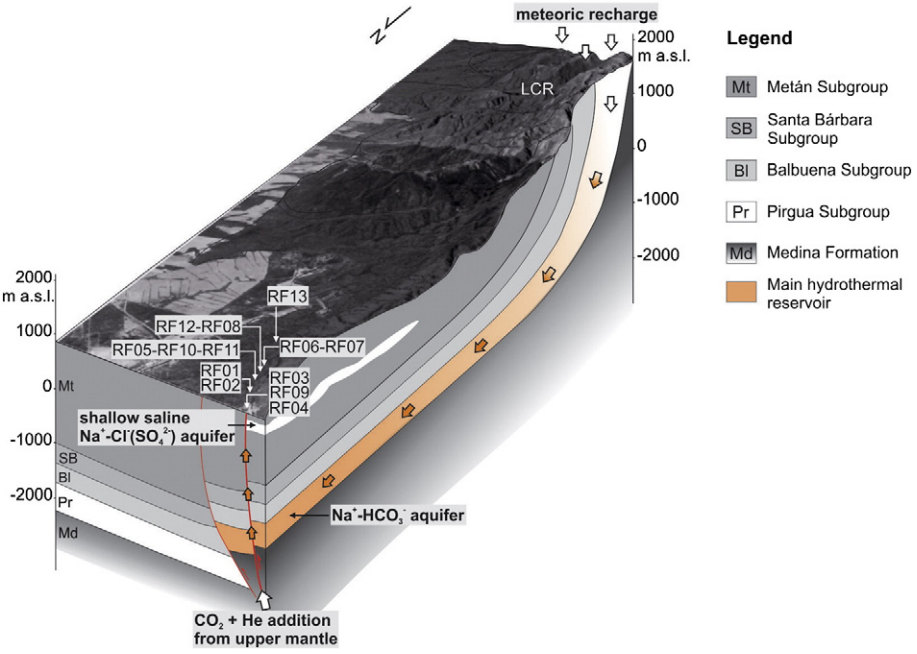

Fig. 11. Three-dimensional conceptual model of underground fluid circulation of RFHS.

results suggest that RFSH can be regarded as one of the most important thermal sites in this sector of the Sub-Andean foreland thrust belt. The heat stored at depth in the extraordinarily large volume of the aquifer hosted in the Pirgua Subgroup can be utilized for different purposes. Firstly, economical benefits can be derived by increasing the thermal tourism and balneology with the construction of new thermal centers or by implementing the already existing structures. Furthermore, the undersaturation in calcite and other salts of the RFSH waters may render the geothermal aquifer suitable for district heating (tele-heating) and cooling by installing appropriate heat exchangers. Other applications for direct or indirect uses, e.g. green-housing, agro-industrial activities should be evaluated in agreement with the local authorities, which should adopt an environmental and economical sustainable policy to exploit the geothermal resource.

Acknowledgments

This work was financially supported by C.U.I.A. (Consorzio Universitario Italiano per l'Argentina), IV Programma di ricerca 2010–2012, coordinator C. Invernizzi, and by the Italian Ministry for Foreign Affairs (Progetto Grande Rilevanza n. 00187, coordinator G. Giordano). We thank Pablo Caffe and Lea di Paolo for useful discussion and helping in the fieldwork. Jose G. Viramonte, Agostina Chiodi and Walter Baez thank INENCO e UNSa-CONICET for the financial and logistic support to this project. Dr. Yuri Taran is warmly thanked for his constructive comments and suggestions that helped the authors to improve an early version of the manuscript

References

Aggarwal, J.K., Palmer, M.R., Bullen, T.D., Arnosson, S., Ragnarsdottir, K.V., 2000. The boron isotope systematic of Icelandic geothermal waters: 1. Meteoric water charged systems. Geochim. Cosmochim. Acta 64, 579–585.

Aggarwal, J., Böhm, F., Foster, G., Halas, S., Hönisch, B., Jiang, S.Y., et al., 2009. How well do non-traditional stable isotope results compare between different laboratories: results from the interlaboratory comparison of boron isotope measurements. J. Anal. Atom. Spectrom. 24, 825–831.

Allmendinger, R.W., Gubbels, T., 1996. Pure and simple shear plateau uplift: Altiplano-Puna, Argentina and Bolivia. Tectonophysics 259, 1–13.

Allmendinger, R.W., Ramos, V.A., Jordan, T.E., Palma, M., Isacks, B.L., 1983. Paleogeography and Andean structural geometry, northwest Argentina. Tectonics 2, 1–16.

Arnórsson, S., 1985. The use of mixing models and chemical geothermometers for estimating underground temperatures in geothermal systems. J. Volcanol. Geotherm. Res. 23, 299–335.

Arnósson, S., Andresdottir, A., 1995. Processes controlling the distribution of boron and chlorine in natural waters in Iceland. Geochim. Cosmochim. Acta 59, 4125–4146.

Barcelona, H., Favetto, A., Peri, V., Pomposiello, C., Ungarelli, C., 2013. The potential of audiomagnetotellurics in the study of geothermal fields: a case study from the northern segment of the La Candelaria Range, northwestern Argentina. J. Appl. Geophys. 88, 83–93.

Bencini, A., 1985. Applicabilità del metodo dell'Azometina-H alla determinazione del Boro nelle acque naturali. Rend. Soc. Ital. Mineral. Petrol. 40, 311–316.

Bercheñi, V.A., 2003. Hidrogeología en la ciudad de Rosario de la Frontera y su relación con la cuenca del Río Rosario. Professional Thesis, Universidad Nacional de Salta, Argentina (in Spanish).

Bernard, B.B., Brooks, J.M., Sackett, W.M., 1978. Light hydrocarbons in recent Texas continental shelf and slope sediments. J. Geophys. Res. 83, 4053–4061.

Bianucci, H., Acevedo, O., Cerdán, J., 1981. Evolución tectosedimentaria del Grupo Salta en la Subcuenca Lomas de Olmedo (provincias de Salta y Formosa). Final Proc. VIII Congreso Geológico Argentino, San Luis, Argentinapp. 159–172 (in Spanish).

Bianucci, H., Homovc, J.F., Acevedo, O.M., 1982. Inversion tectonica y plegamientos resultantes en la comarca Puesto Guardian-Dos puntitas. Depto. Orán, Provincia de Salta. Final Proc. I Congreso Nacional de Hicrocarburos, Buenos Aires, Argentinapp. 23–30 (in Spanish).

Bossi, G., 1969. Geología y estratigrafía del sector sur del Valle del Choromoro. Acta Geol. Lilloana 10 (2), 17–64 (in Spanish).

Carmona, V., Pueyo, J.J., Taberner, C., Chong, G., Thirlwall, M., 2000. Solute inputs in the Salar de Atacama (N. Chile). J. Geochem. Explor. 69, 449–452.

Carrera, N., Muñoz, J.A., Sábat, F., Mon, R., Roca, E., 2006. The role of inversion tectonics in the structure of the Cordillera Oriental (NW Argentinean Andes). J. Struct. Geol. 28, 1921–1932. http://dx.doi.org/10.1016/j.jsg.2006.07.006.

Chiodini, G., Allard, P., Caliro, S., Parello, F., 2000. ^{18}O exchange between steam and carbon dioxide in volcanic and hydrothermal gases: implications for the source of water. Geochim. Cosmochim. Acta 64, 2477–2488.

Coleman, M.L., Sheperd, T.J., Rouse, J.E., Moore, G.R., 1982. Reduction of water with zinc for hydrogen isotope analysis. Anal. Chem. 54, 993–995.

Comínguez, A., Ramos, V., 1995. Geometry and seismic expression of the Cretaceous Salta Rift System, Northwestern Argentina. In: Tankard, A., Suárez, R., Welsink, H. (Eds.), Petroleum basins of South America. American Association of Petroleum Geologists Memoirs, pp. 325–340.

Cortecci, G., Boschetti, T., Mussi, M., Herrera Lameli, C., Mucchino, C., Barbieri, M., 2005. New chemical and original isotopic data on waters from El Tatio geothermal field, northern Chile. Geochem. J. 39, 547–571.

Cristallini, E., Cominguez, A., Ramos, V., 1997. Deep structure of the Metan-Guachipas region: tectonic inversion in Northwestern Argentina. J. S. Am. Earth Sci. 10, 403–421.

Dapeña, C., Panarello, H., 2011. Composición isotópica de las precipitaciones en el Noroeste Argentino. Final Proc. VII Congreso Argentino de Hidrogeología and V Seminario Hispano-Latinoamericano Sobre Temas Actuales de la Hidrología Subterránea, Salta, Argentinapp. 385–392 (in Spanish).

Di Paolo, L., Aldega, L., Corrado, S., Giordano, G., Invernizzi, C., 2012. Modelling of organic and inorganic paleo-thermal indicators to constrain the evolution of the geothermal system of Rosario de La Frontera (La Candelaria Ridge, NW Argentina): a new tool for geothermal exploration. Rend. Online Soc. Geol. Ital. 21, 807–808.

Epstein, S., Mayeda, T.K., 1953. Variation of the $^{18}O/^{16}O$ ratio in natural waters. Geochim. Cosmochim. Acta 4, 213–224.

Evans, W.C., White, L.D., Rapp, J.B., 1998. Geochemistry of some gases in hydrothermal fluids from the southern Juan de Fuca ridge. J. Geophys. Res. 15, 305–313.

Fiedler, K., 2001. Die kretazisch-alttertiaere Entwicklung des suedlichen Potosi-Beckens (Suedbolivien). PhD Thesis, Freie Universitaet Berlin, Fachbereich Geowissenschaften, Alemania (in German).

Galli, C.I., Hernández, R., 1999. Evolución de la Cuenca de Antepaís desde la zona de la Cumbre Calchaquí hasta la Sierra de Santa Bárbara, Eoceno inferior-Mioceno medio, provincia de Salta, Argentina. Acta Geol. Hisp. 34 (2), 167–184 (in Spanish).

Galli, C., Hernández, R., Reynolds, J., 1996. Análisis paleoambiental y ubicación geocronológica del Subgrupo Metán (Grupo Orán, Neógeno) en el río Piedras, Departamento Metán, Salta, Argentina. Boletín de Informaciones Petroleras, Tercera Serie, Buenos Aires, Argentina. 46 pp. 98–107 (in Spanish).

Galliski, M., Viramonte, J.G., 1988. The Cretaceous paleorift in northwestern Argentina: a petrologic approach. J. S. Am. Earth Sci. 1, 329–342.

Gebhard, J., Guidice, A., Gascon, J., 1974. Geología de la comarca entre el Río Juramento y Arroyo las Tortugas, provincias de Salta y Jujuy. Rev. Asoc. Geol. Argent. 29, 359–375 (in Spanish).

Giggenbach, W., 1988. Geothermal solute equilibria, derivation of Na–K–Mg–Ca geoindicators. Geochim. Cosmochim. Acta 52, 2749–2765.

Giggenbach, W.F., 1991. Chemical techniques in geothermal exploration. Application of Geochemistry in Geothermal Reservoir Development.UNITAR, NewYork, pp. 253–273.

Giggenbach, W., Goguel, R., 1989. Collection and analysis of geothermal and volcanic water and gas discharges, unpublished report. Chemistry Division. Department of Scientific and Industrial Research, Petone, New Zealand, p. 81.

Gómez Omil, R.J., Boll, A., Hernandez, R.M., 1989. Cuenca cretácico-terciaria del Noroeste argentino (Grupo Salta). In: Chebli, G.A., Spalletti, L.A. (Eds.), Cuencas Sedimentarias Argentinas. Serie de Correlación Geológica. Universidad Nacional de Tucumán, pp. 43–64 (in Spanish).

Gonfiantini, R., Roche, M.-A., Olivry, J.-C., Fontes, J.-C., Zuppi, G.M., 2001. The altitude effect on the isotopic composition of tropical rains. Chem. Geol. 181, 147–167.

Grier, M., Salfity, J., Allmendiger, R.W., 1991. Andean reactivation of the Cretaceous Salta rift, northwestern Argentina. J. S. Am. Earth Sci. 4, 351–372.

Hain, M.P., Strecker, M.R., Bookhagen, B., Alonso, R.N., Pingel, H., Schmitt, A.K., 2006. Neogene to Quaternary broken foreland formation and sedimentation dynamics in the Andes of NW Argentina (25°S). Tectonics 30, TC2006. http://dx.doi.org/10.1029/2010TC002703.

Hilton, D.R., Fischer, T.P., Marty, B., 2002. Noble gases and volatile recycling at subduction zones. Rev. Mineral. Geochem. 47, 319–370.

Hoefs, J., 2008. Stable Isotope Chemistry. Springer, Berlin, New York, p. 260.

Inguaggiato, S., Rizzo, A., 2004. Dissolved helium isotope ratios in ground-waters: a new technique based on gas-water re-equilibration and its application to a volcanic area. Appl. Geochem. 19, 665–673.

Invernizzi, C., Pierantoni, P.P., Chiodi, A., Maffucci, R., Corrado, S., Báez, W., Tassi, F., Giordano, G., Viramonte, J.G., 2014. Preliminary assessment of the geothermal potential of Rosario de la Frontera area (Salta, NW Argentina): insight from hydrogeological, hydro-geochemical and structural investigations. J. S. Am. Earth Sci. 54, 20–36.

Javoy, M., Pineau, F., Allegre, C.J., 1982. Carbon geodynamic cycle. Nature 300, 171–173.

Jordan, T., Isacks, B., Allmendinger, R.W., Brewer, J.A., Ramos, V.A., Ando, C.J., 1983. Andean tectonics related to geometry of subducted Nazca plate. Geol. Soc. Am. Bull. 94, 341–361.

Kasemann, S.A., Meixner, A., Erzinger, J., Viramonte, J.G., Alonso, R.N., Franz, G., 2004. Boron isotope composition of geothermal fluids and borate minerals from salar deposits (central Andes/NW Argentina). J. S. Am. Earth Sci. 16, 685–697.

Kley, J., Monaldi, C.R., 1998. Tectonic shortening and crustal thickness in the Central Andes: how good is the correlation? Geology 26, 723–726.

Kley, J., Monaldi, C., 2002. Tectonic inversion in the Santa Barbara System of the central Andean foreland thrust belt, northwestern Argentina. Tectonics 21, 1111–1118.

Kress, P.R., 1995. Tectonic inversion of the Subandean Foreland—a combined geophysical and geological approach. Berl. Geowiss. Abh. 23, 120.

Leybourne, M.I., Cameron, E.M., Reich, M., Palacios, C., Faure, K., Johannesson, K.H., 2013. Stable isotopic composition of soil calcite (O, C) and gypsum (S) overlying Cu deposits in the Atacama Desert, Chile: implications for mineral exploration, salt sources, and paleoenvironmental reconstruction. Appl. Geochem. 29, 55–72.

Maffucci, R., Bigi, S., Corrado, S., Di Paolo, L., Chiodi, A., 2012. Fracture modeling applied to the geothermal system potential reservoir of Rosario de La Frontera (La Candelaria Ridge, NW Argentina). Rend. Online Soc. Geol. Ital. 21, 829–831.

Maffucci, R., Bigi, S., Chiodi, A., Corrado, S., Giordano, G., Di Paolo, L., 2013. Reconstruction of a "Discrete Fracture Network" in the geothermal reservoir of Rosario de La Frontera (La Candelaria Ridge, Salta province, NW Argentina). Final Proc. European Geothermal Congress, Pisa, Italy.

Mamyrin, B.A., Tolstikhin, I.N., 1984. Helium isotopes in nature. In: Fyfe, W.S. (Ed.), Development in Geochemistry. Elsevier, Amsterdam, p. 274.

Marquillas, R., Del Papa, C., Sabino, I.F., 2005. Sedimentary aspects and paleoenvironmental evolution of a rift basin: Salta Group (Cretaceous–Paleogene), northwestern Argentina. Int. J. Earth Sci. 94, 94–113.

Martini, M., Cellini Legittimo, P., Piccardi, G., Giannini, L., 1984. Low temperature manifestations in volcanic areas. Rend. Soc. Ital. Mineral. Petrol. 39, 401–405.

Marty, B., Jambon, A., 1987. $C/^3He$ fluxes from the solid Earth: implications for carbon geodynamics. Earth Planet. Sci. Lett. 83, 16–26.

Mingramm, A., Russo, A., Pozzo, A., Cazau, L., 1979. Sierras Subandinas. In: Turner, J. (Ed.), Geología Regional Argentina. Academia Nacional de Ciencias Córdoba, Argentina, pp. 95–138.

Moreno Espelta, C., Viramonte, J.G., Arias, J., 1975. Geología del área termal de Rosario de la Frontera y sus posibilidades geotérmicas. Final Proc. II Congreso Ibero-Americano de Geología Económica, Buenos Aires, Argentinapp. 543–548 (in Spanish).

Parkhurst, D.L., Appelo, C.A.J., 1999. User's guide to PHREEQC (version 2)—a computer program for speciation, batch-reaction, one-dimensional transport, and inverse geochemical calculations. U.S. Geological Survey Water-Resources Investigations Report 99–4259p. 312.

Pesce, A., Miranda, F., 2003. Catálogo de manifestaciones termales de la República Argentina. Región Noroeste. vol. I. SEGEMAR, Buenos Aires, Argentina, p. 165.

Poreda, R.J., Craig, H., 1989. Helium isotope ratios in circum-Pacific volcanic arcs. Nature 338, 473–478.

Ramos, V.A., 2008. The basement of the Central Andes: the Arequipa and related terranes. Annu. Rev. Earth Planet. Sci. 36, 289–324.

Reyes, F., Salfity, J., 1973. Consideraciones sobre la estratigrafía del Cretácico (Subgrupo Pirgua) del noroeste Argentino. Final Proc. V Congreso Geológico Argentino, Córdoba, Argentinapp. 355–385 (in Spanish).

Reynolds, J.H., Galli, C.J., Hernandez, R.M., Idleman, B.D., Kotila, J.M., Hilliard, R.V., Naeser, C.W., 2000. Middle Miocene tectonic development of the Transition Zone, Salta Province, northwest Argentina: magnetic stratigraphy from the Metán Subgroup, Sierra de González. Geol. Soc. Am. Bull. 112, 1736–1751.

Rollinson, H., 1993. Using Geochemical Data. Longman, London, UK, p. 352.

Salfity, J., Marquillas, R., 1994. Tectonic and sedimentary evolution of the Cretaceous–Eocene Salta Group, Argentina. In: Salfity, J. (Ed.), Cretaceous Tectonics of the Andes. Earth Evolution Sciences. Friedrich Vieweg and Sohn, Brunswick, United States of America, pp. 266–315.

Salfity, J.A., Monaldi, C.R., Marquillas, R.A., Gonzáles, R.E., 1993. La inversión tectónica del Umbral de los Gallos en la cuenca del Grupo Salta durante la Fase Incaica. Final Proc. XII Congreso Geológico Argentino and II Congreso de Exploración de Hidrocarburos, Mendoza, Argentinapp. 200–210 (in Spanish).

Sano, Y., Wakita, H., 1985. Geographical distribution of $^3He/^4He$ in Japan: implications for arc tectonics and incipient magmatism. J. Geophys. Res. 90, 8729–8741.

Schoell, M., 1980. The hydrogen and carbon isotopic composition of methane from natural gases of various origins. Geochim. Cosmochim. Acta 44, 649–661.

Seggiaro, R., Aguilera, N., Gallardo, E., Ferreti, J., 1995. Structure and geothermal potential of the Rosario de la Frontera thermal area, Salta. Argentina. Final Proc. World Geothermal Congress, Florence, Italy. 2 pp. 764–767.

Seggiaro, R., Aguilera, N., Ferretti, J., Gallardo, E., 1997. Estructura del área geotérmica de Rosario de la Frontera, Salta, Argentina. Final Proc. VIII Congreso Geológico Chileno, Antofagasta, Chilepp. 390–394 (in Spanish).

Spiro, B., Chong, G., 1996. Origin of sulfate in the Salar de Atacama and the Cordillera de la Sal, initial results of an isotopic study. Final Proc. III International Symposium on Andean Geodynamics (ISAG), Saint Malo, Francepp. 703–707.

Tassi, F., Vaselli, O., Luchetti, G., Montegrossi, G., Minissale, A., 2008. Metodo per la determinazione dei gas disciolti in acque naturali. Internal Report CNR-IGG, n. p. 10 (10420).

Tassi, F., Fiebig, J., Vaselli, O., Nocentini, M., 2012. Origins of methane discharging from volcanic-hydrothermal, geothermal and cold emissions in Italy. Chem. Geol. 310, 36–48.

Tonani, F., 1970. Geochemical methods of exploration for geothermal energy. Geothermics 2, 492–515.

Turner, J., 1959. Estratigrafía del cordón de Escaya y de la Sierra de Rinconada (Jujuy). Rev. Asoc. Geol. Argent. 13, 15–39 (in Spanish).

Vaselli, O., Tassi, F., Montegrossi, G., Capaccioni, B., Giannini, L., 2006. Sampling and analysis of volcanic gases. Acta Volcanol. 18, 65–76.

Whitfield, M., 1978. Activity coefficients in natural waters. In: Pytkowicz, R.M. (Ed.), Activity Coefficients in Electrolyte Solutions. CRC Press, Boca Raton, FL, pp. 153–300.

Whitman, D., Isacks, B.L., Kay, S.M., 1996. Lithospheric structure and along-strike segmentation of the Central Andean Plateau: seismic, magmatism, flexure, topography and tectonics. Tectonophysics 259, 29–40.

Yardley, B.W., Bodnar, R.J., 2014. Fluids in the continental crust. Geochem. Perspect. 3, 127.

Zhang, J., Quay, P.D., Wilbur, D.O., 1995. Carbon isotope fractionation during gas–water exchange and dissolution of CO_2. Geochim. Cosmochim. Acta 59, 107–114.